LW1 PSF: wider than expected?

- Resampled PSFs are used to estimate their FWHM

- LW1, LW3 and LW10 seem to deviate from the theoretical FWHM

- After correction of the effect of the filter band width and the spectrum of the calibration star, LW1 remains wider than the predicted FWHM

- It does NOT seem to come from the difraction limit of the telescope

- Filter leak? Crucial transient effect?

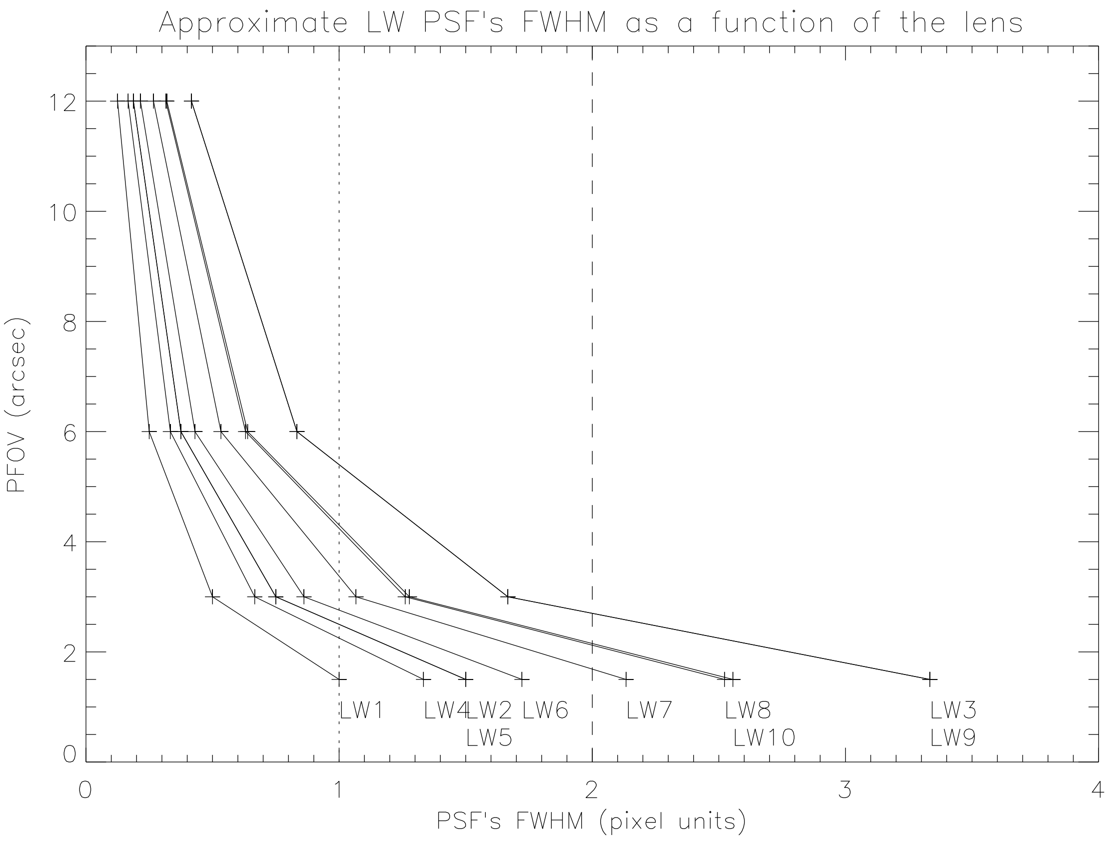

Figure 1: Size of a point source with respect to the pixel size of LW channel

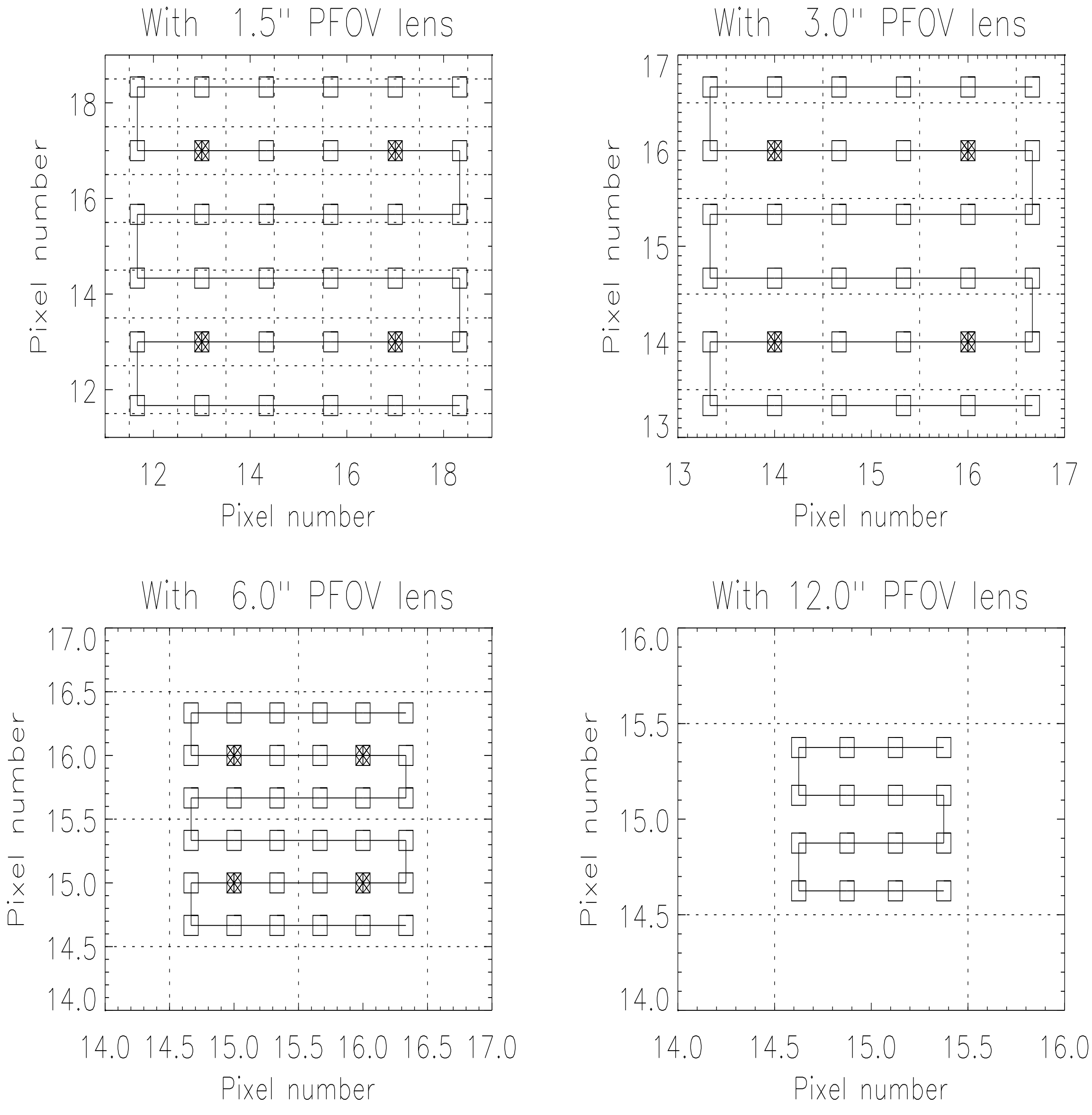

Figure 2: Point source displacement along a scanning raster

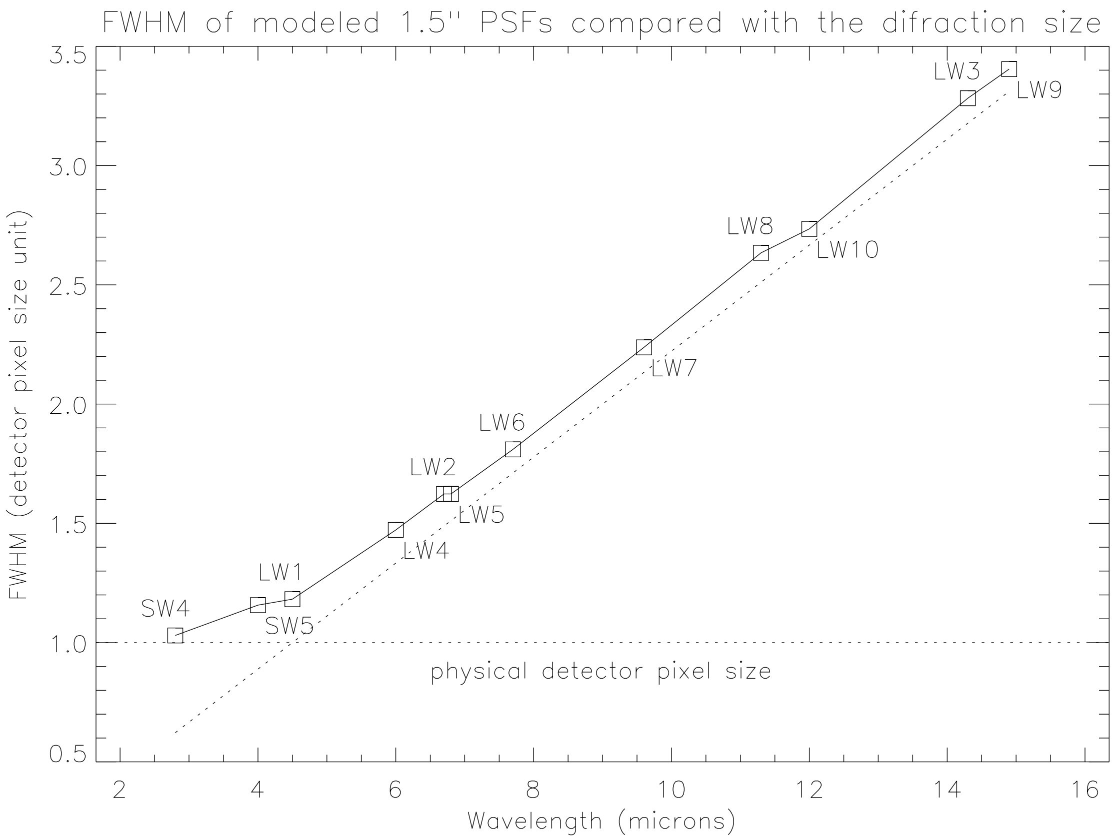

Figure 3: FWHMs of the modeled PSFs. The dashed line is the Airy disk diameter following ISOCAM Observer's Manual.

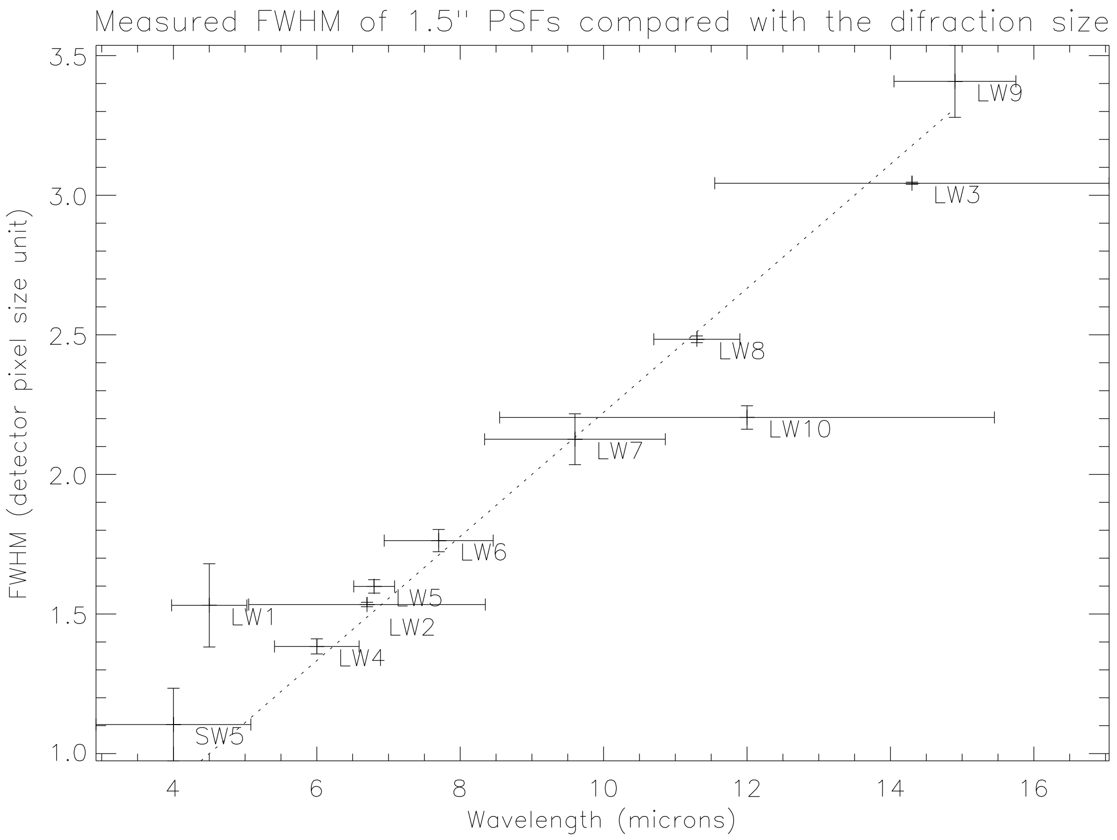

Figure 4: FWHMs of the measured PSF. The dashed line is the Airy disk diameter following ISOCAM Observer's Manual. The horizontal error bars indicate the bandwidth of each filter.

Table 1: Effective wavelengths of the filters for the spectral index of -4

SW	$\lambda_{\rm ref}$	$\lambda_{\rm eff}$	LW	$\lambda_{\rm ref}$	$\lambda_{\rm eff}$
SW4	2.8	2.75	LW1	4.5	4.44
SW7	3.0	3.04	LW4	6.0	5.94
SW2	3.3	6.36	LW2	6.7	6.36
SW1	3.6	3.51	LW5	6.8	6.77
SW6	3.7	3.68	LW6	7.7	7.66
SW9	3.9	3.87	LW7	9.6	9.49
SW5	4.0	3.85	LW8	11.3	11.29
SW8	4.05	4.05	LW10	12.0	10.67
SW11	4.26	4.22	LW3	14.3	13.99
SW3	4.5	4.37	LW9	14.9	14.85
SW10	4.6	4.62			

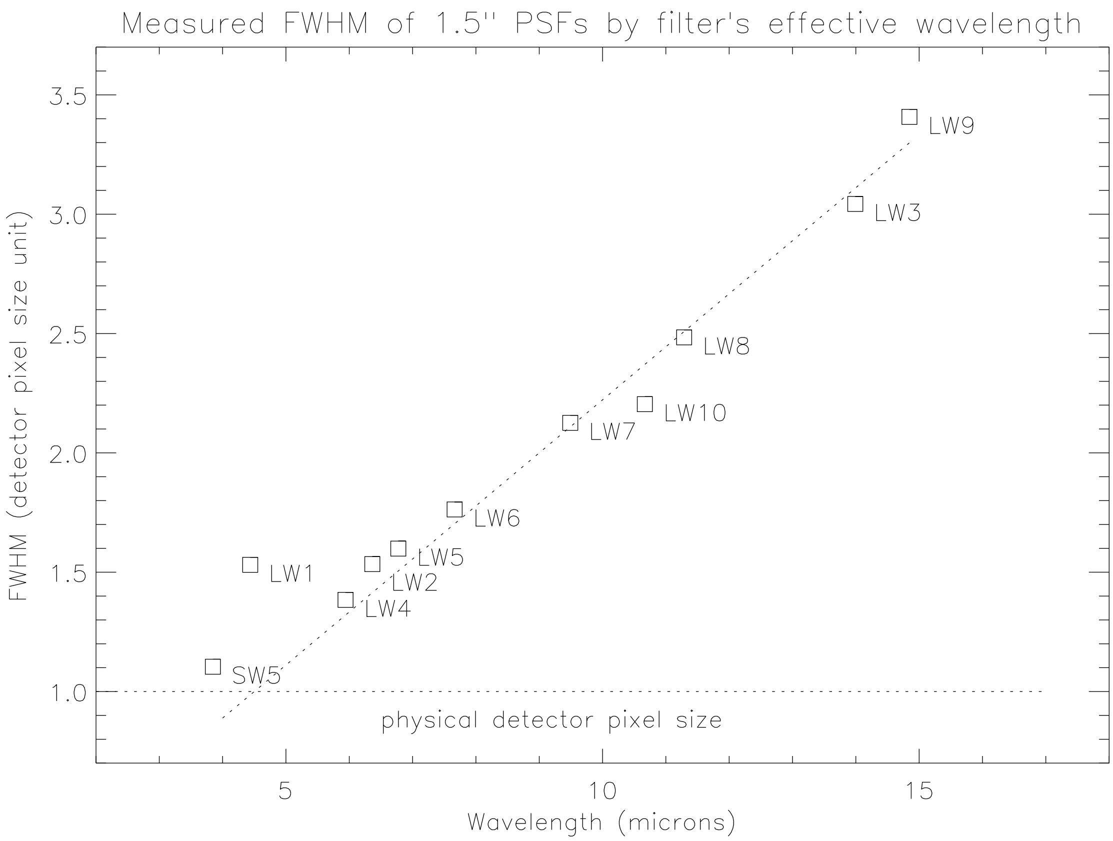

Figure 5: FWHMs of the measured PSF. The dashed line is the Airy disk diameter following ISOCAM Observer's Manual. The reference wavelength of each filter is replaced by its effective wavelength using a spectral index of -4: λ^{-4}

Undesirable light in CAM images

Stray light

- Observation around NML-Cygnus: radially oriented 6 rasters

- At the closest raster points, 4.6 arcmin from the detector center, the stray light reaches 10^{-6} to 10^{-5} of the source flux as was predicted by the optical model simulations before the launch

- The ghosts give a stronger contribution in the undesirable light

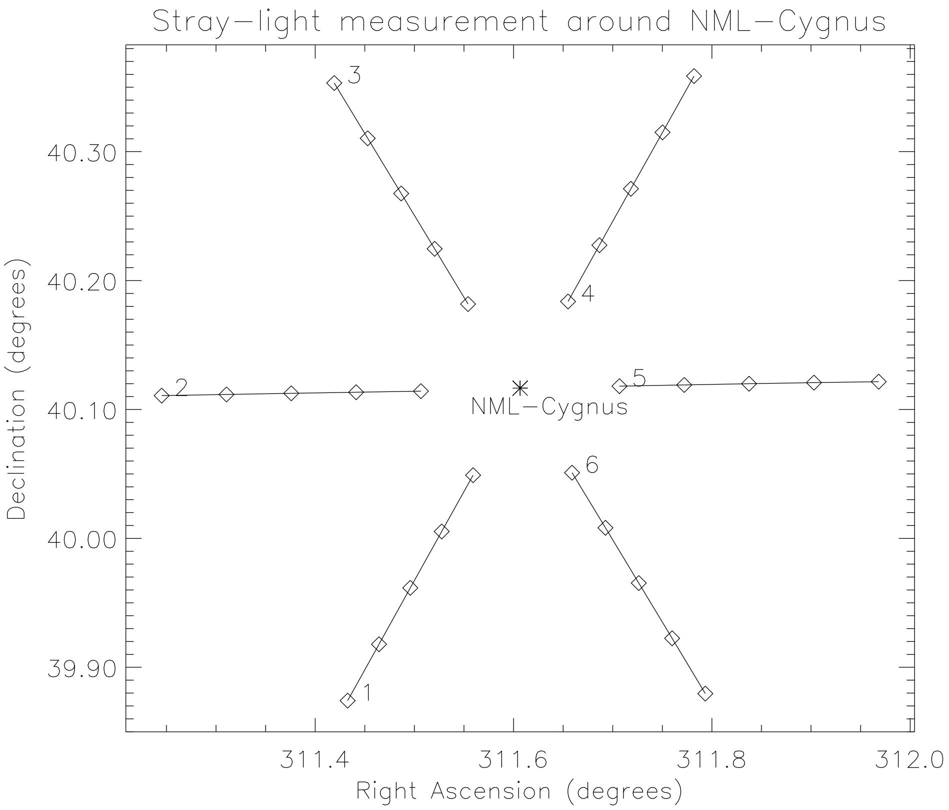

Figure 6: Raster scans used for the stray-light measurement in Rev.46

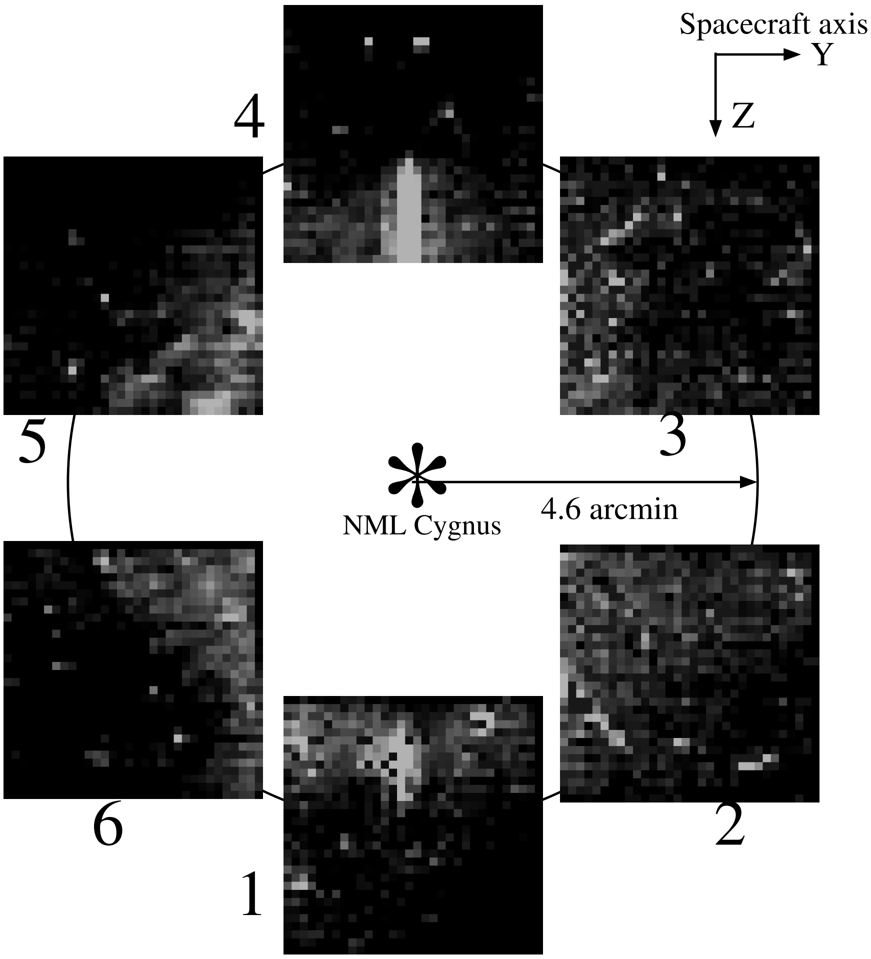

Figure 7: Stray-light measurement with NML Cygnus

Ghosts

- Filter tilt displaces the ghosts but not enough in 6 and 12 arcsec filter images

- 2 ghosts in 6 arcsec CVF images

- Big pupil image in 3 arcsec CVF images

- Discontinuous behaviour of a CVF ghost

- Very discontinuous ghost behaviour in 6 arcsec filter images

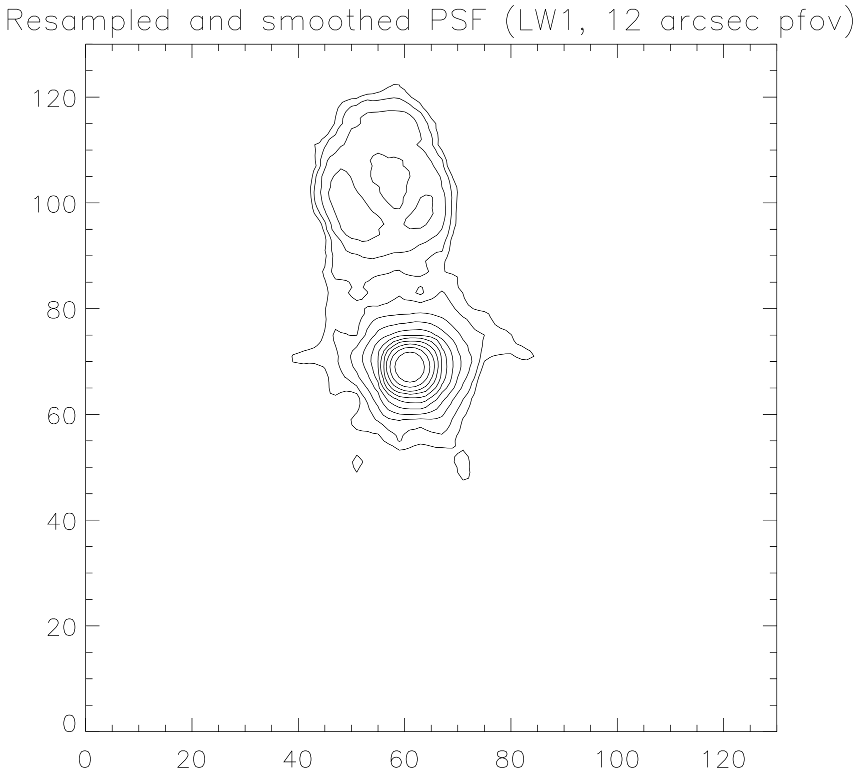

Figure 8: Primary ghost image beside a point source (LW1 with 12 arcsec pfov)

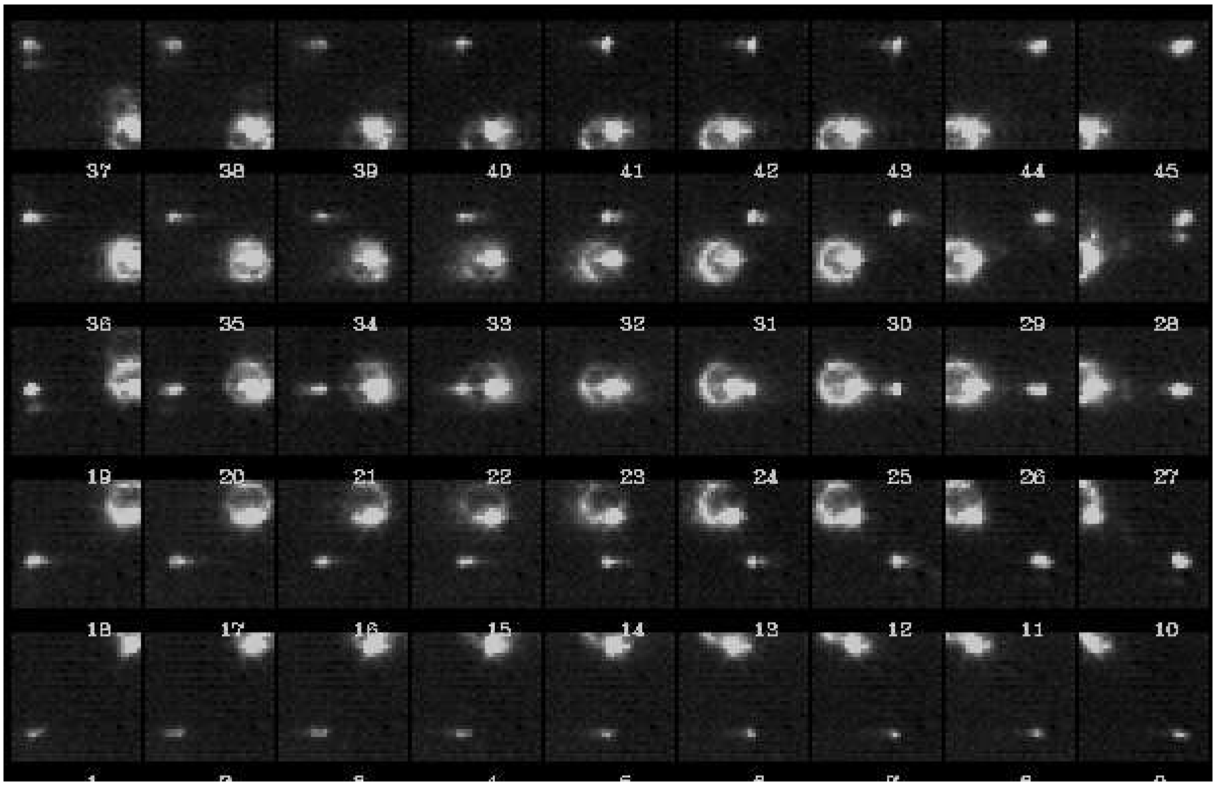

Figure 9: Global behaviour of ghosts when a point source moves over the detector (CVF at 7 μm with 6 arcsec PFOV in Rev. 531)

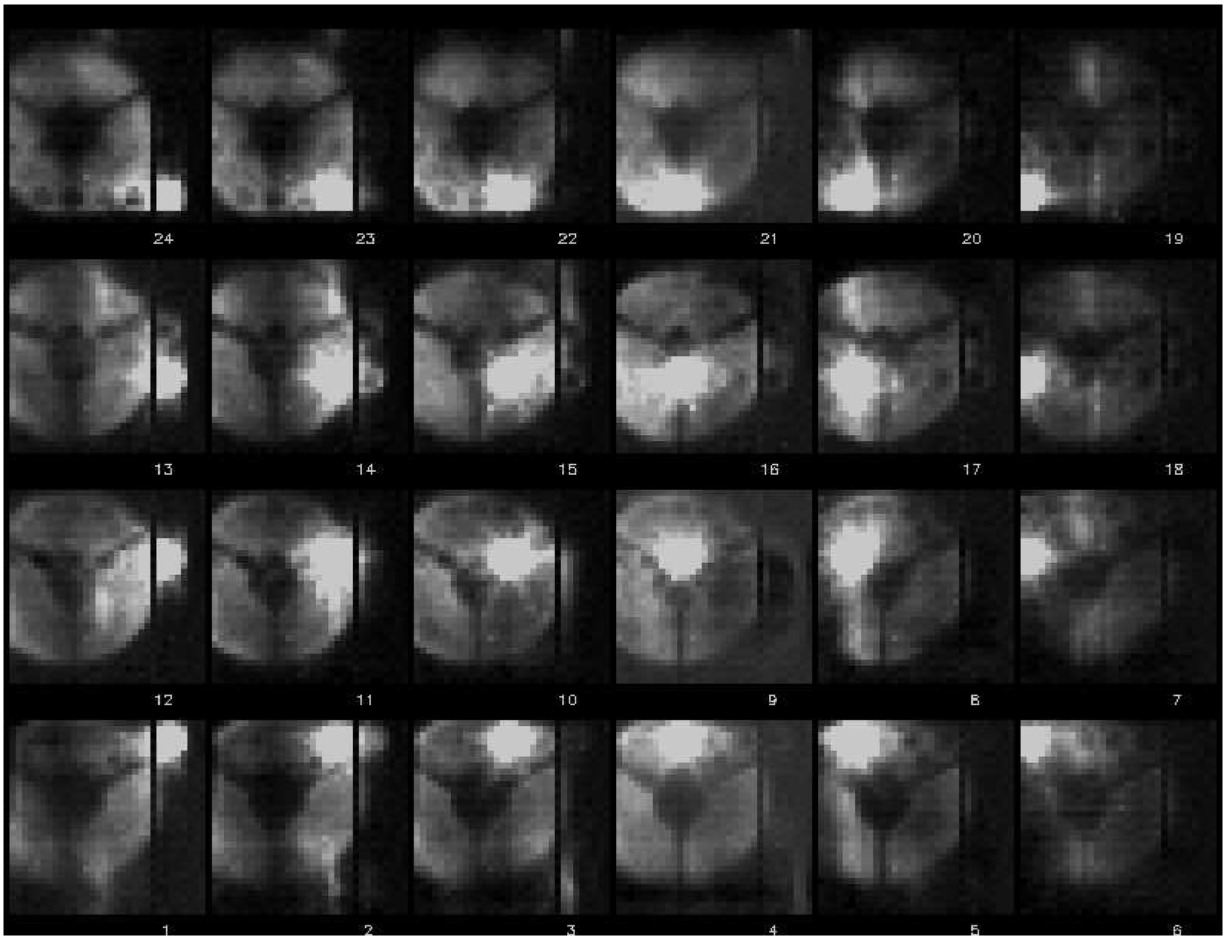

Figure 10: Global behaviour of ghosts when a point source moves over the detector (CVF at 5 μm with 3 arcsec PFOV in Rev. 730)

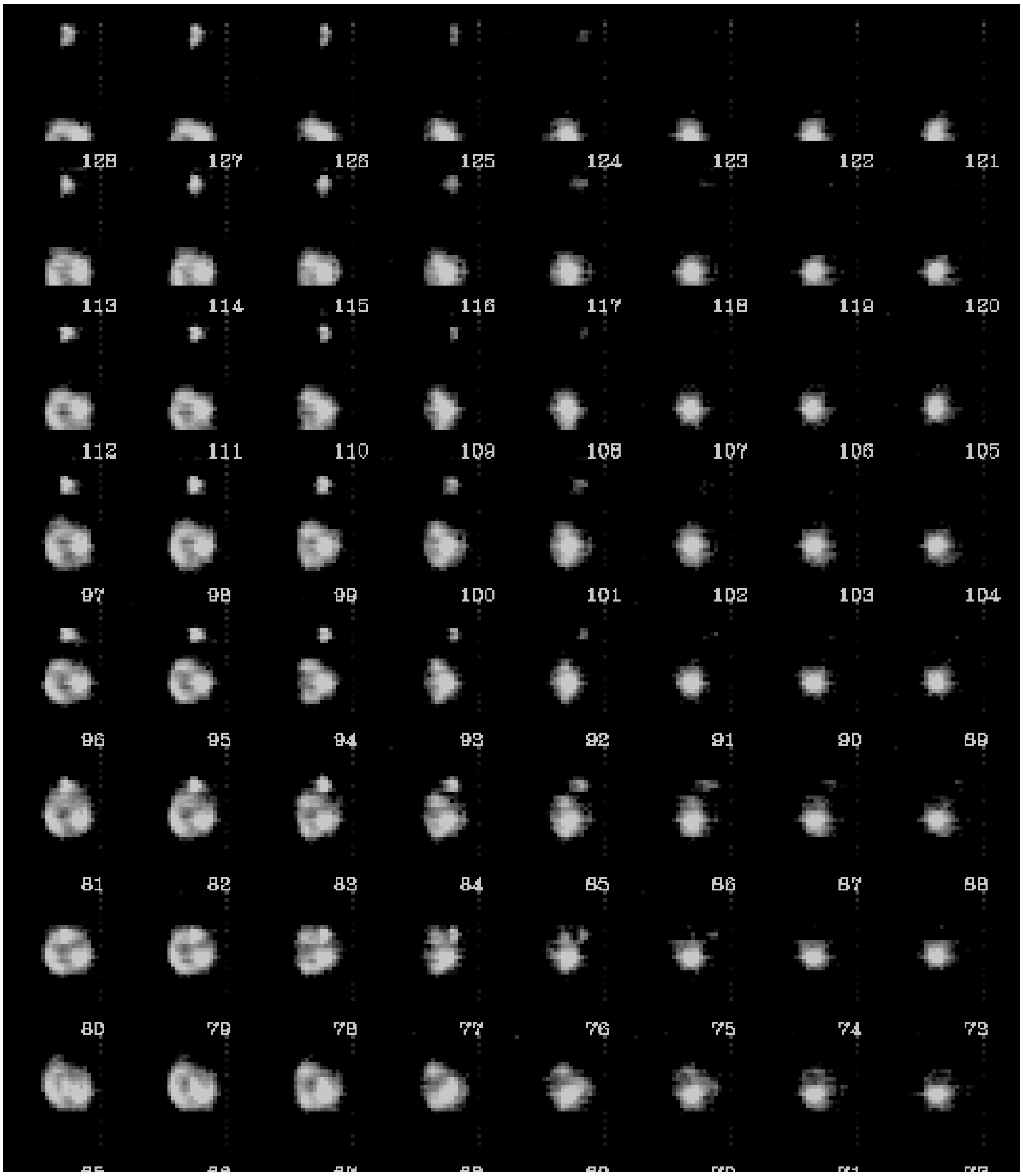

Figure 11: Discontinuous behaviour of ghosts when a point source moves over the detector (CVF at 5 μm with 6 arcsec PFOV in Rev. 740)

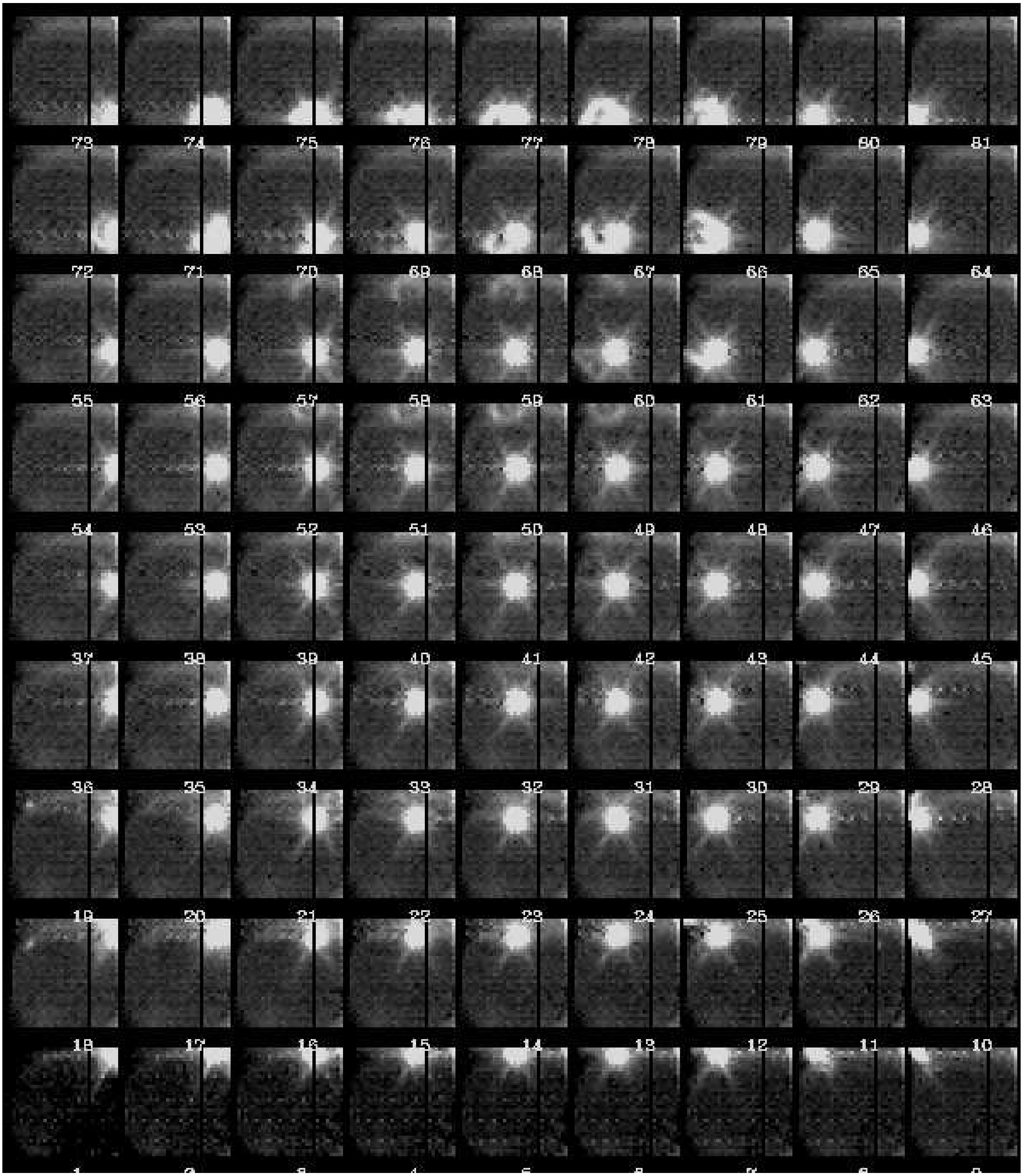

Figure 12: Global behaviour of ghosts when a point source moves over the detector (LW3 filter at 15 μm with 6 arcsec PFOV in Rev. 576)

Optical model using ASAP
Licence of IAS (Y.Longval)

- Optical elements of the telescope: Primary, Secondary, Spiders and pyramidal mirror

- Optical elements of the ISOCAM: field mirror, filters, lenses and detector plus simplified filter mount

- The 2 major ghosts observed in the CVF images with 6 arcsec pfov lens are well identified as multi-reflections in the camera

- The first order correction of the ghosts may be considered as a most direct deconvolution

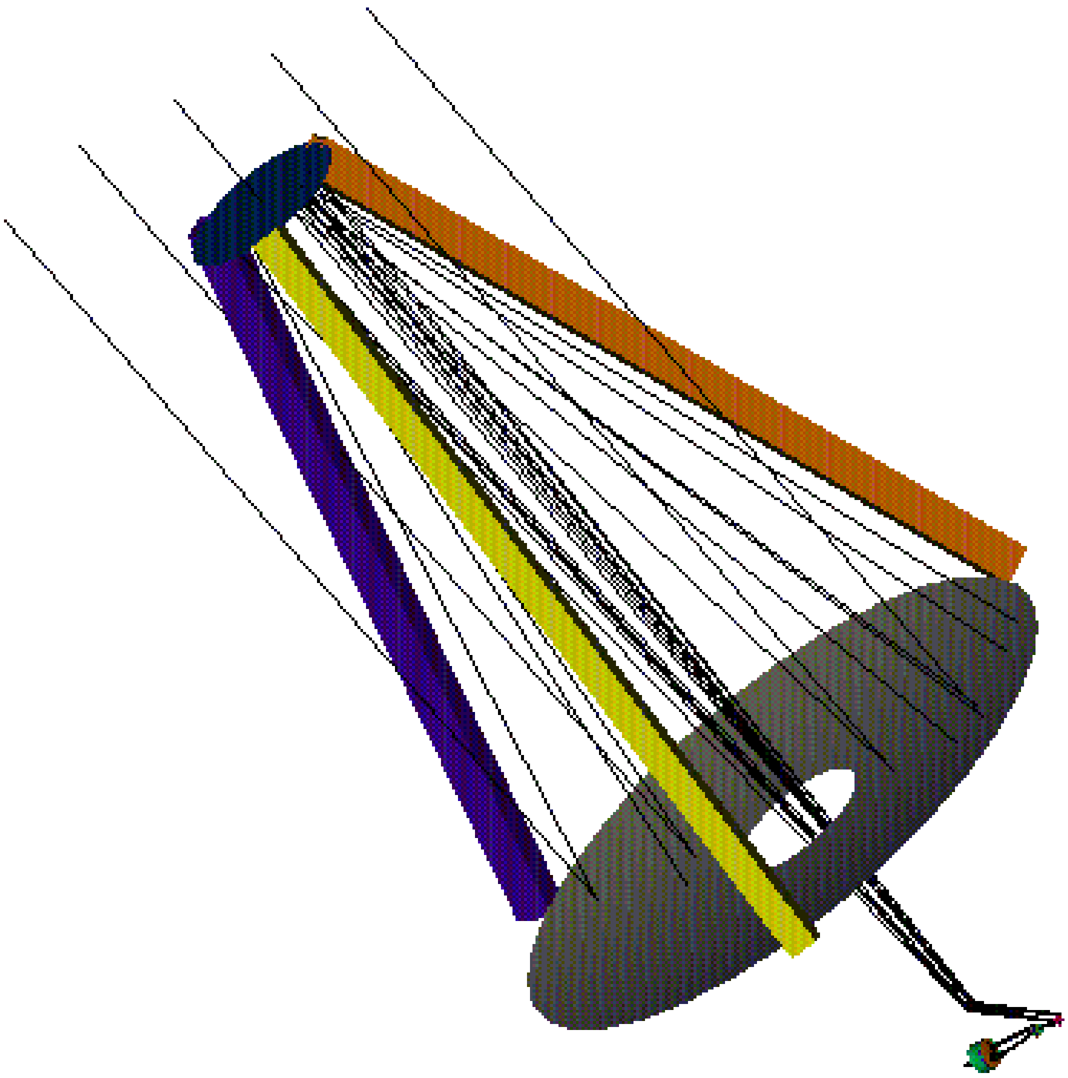

Figure 13: Modeled optical elements of the ISO telescope

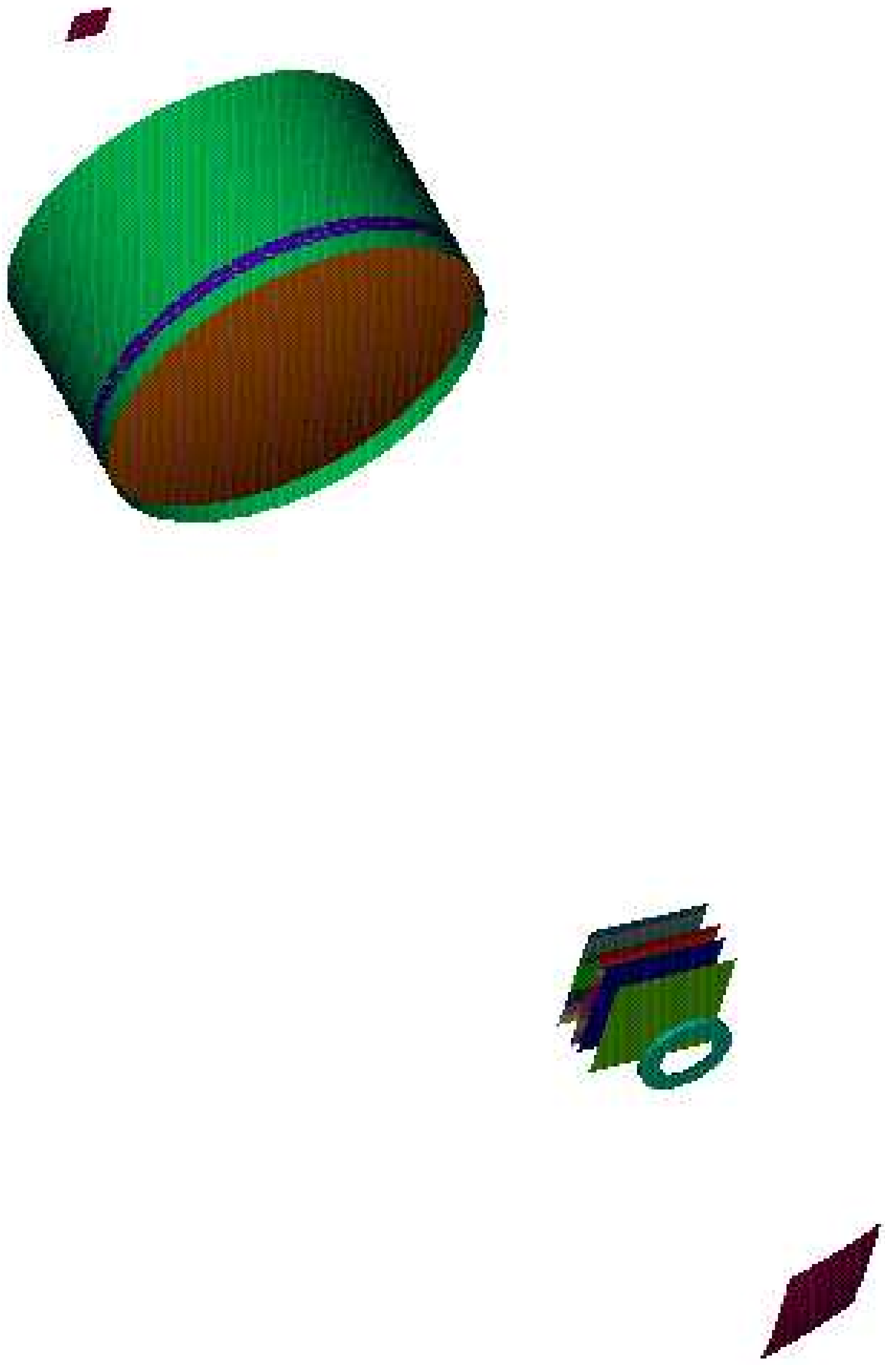

Figure 14: Modeled optical elements of the ISOCAM

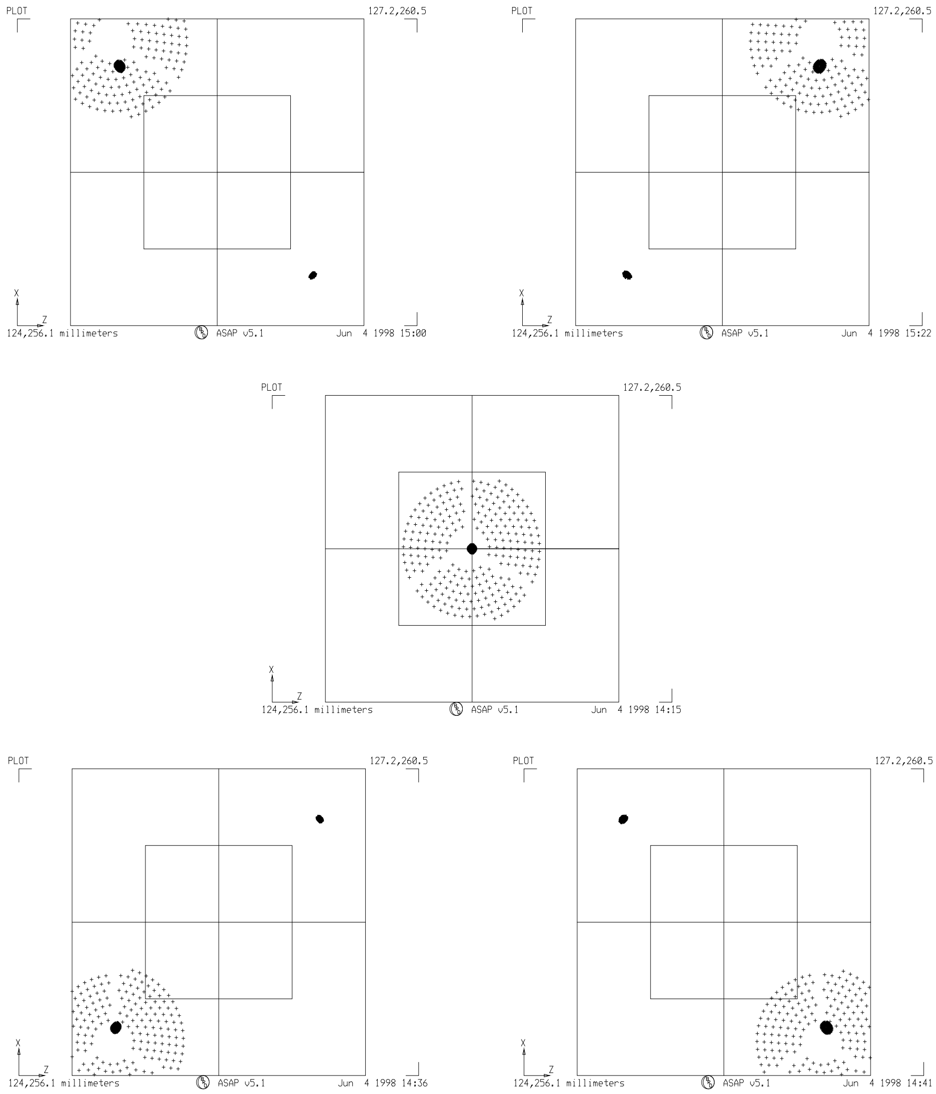

Figure 15: With a CVF and 6 arcsec FPOV lens, the primary ghost is always around the point source whereas the secondary ghost is point-like and is located near the symmetrical point of the source with respect to the detector centre.

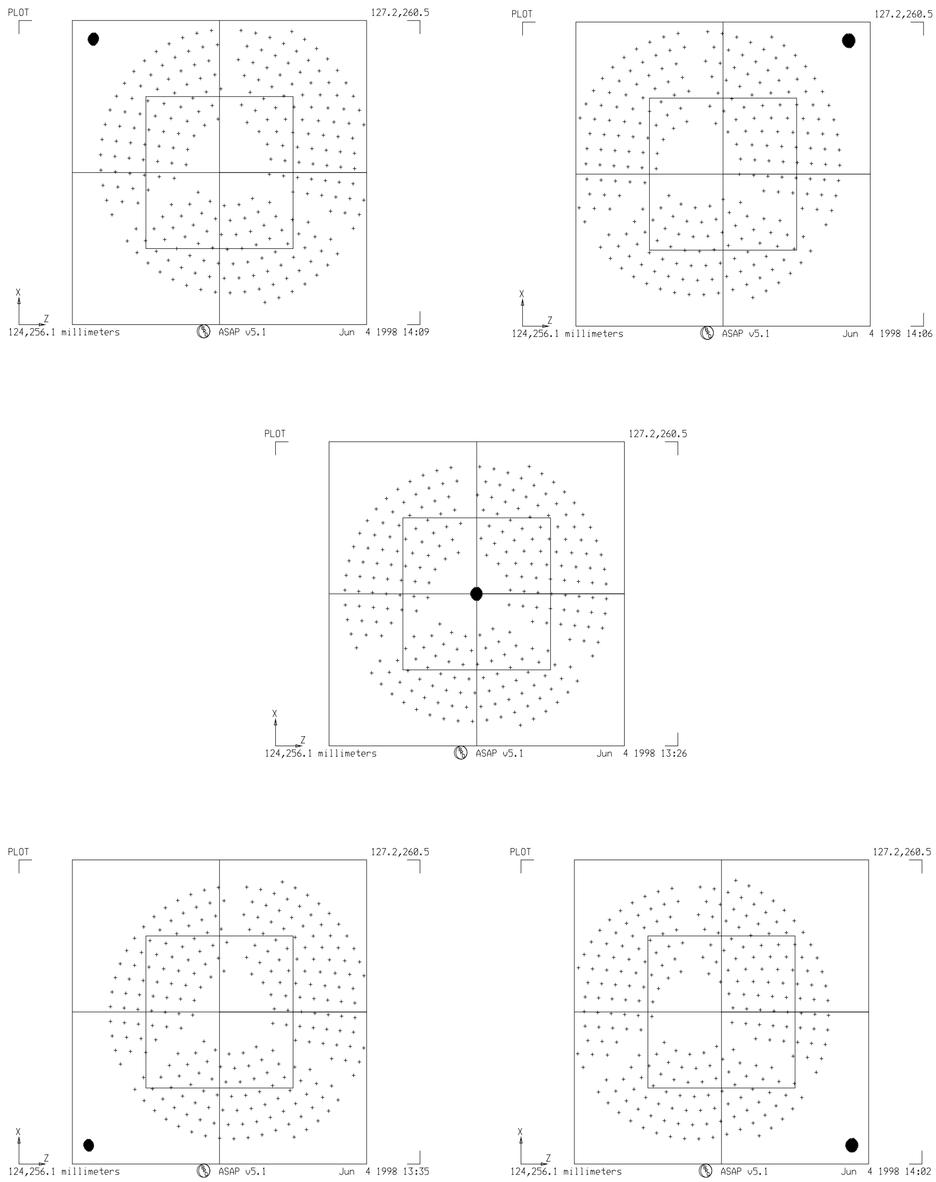

Figure 16: With a CVF and 3 arcsec FPOV lens, the primary ghost covers a large part of the detector and its location depends very little on that of the point source.

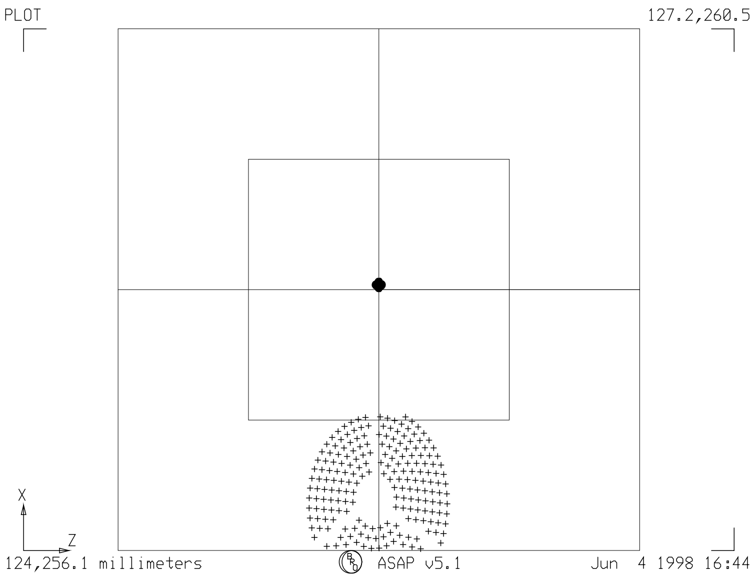

Figure 17: The primary ghost for a filter is displaced toward the positive Z-axis due to its tilt of 5°. With 12 arcsec FPOV lens a large fraction of it is seen in a elliptical form.

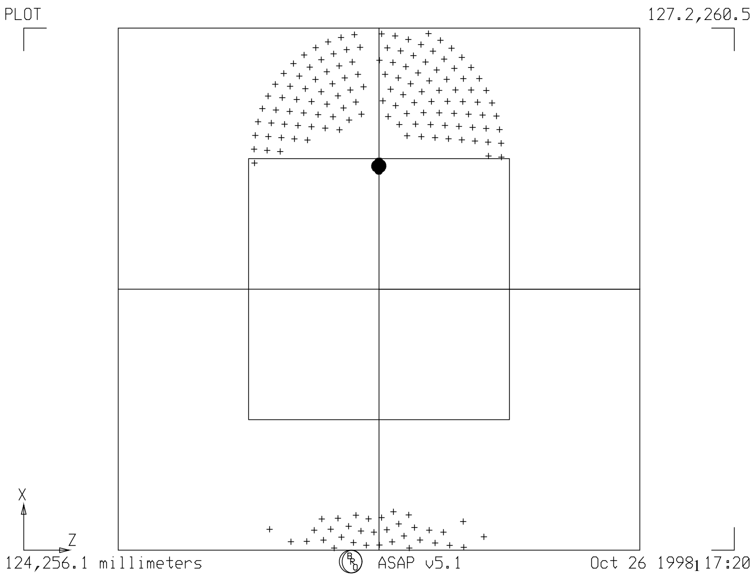

Figure 18: The discontinuous behaviour of the ghosts with a filter at 6 arcsec lens is qualitatively reproduced in the optical model.

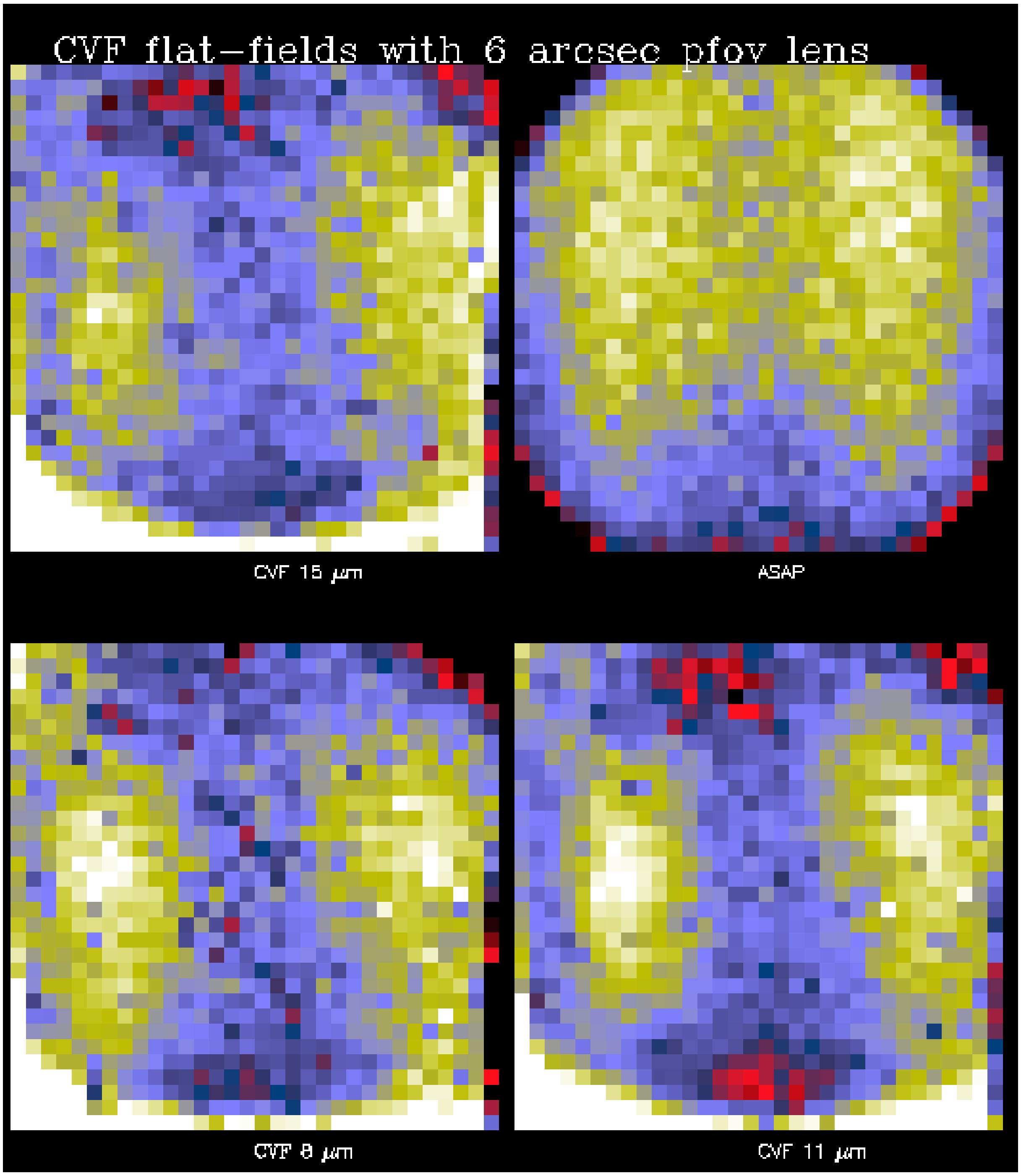

Figure 19: Comparison between measured and modeled optical flat-field for a CVF.

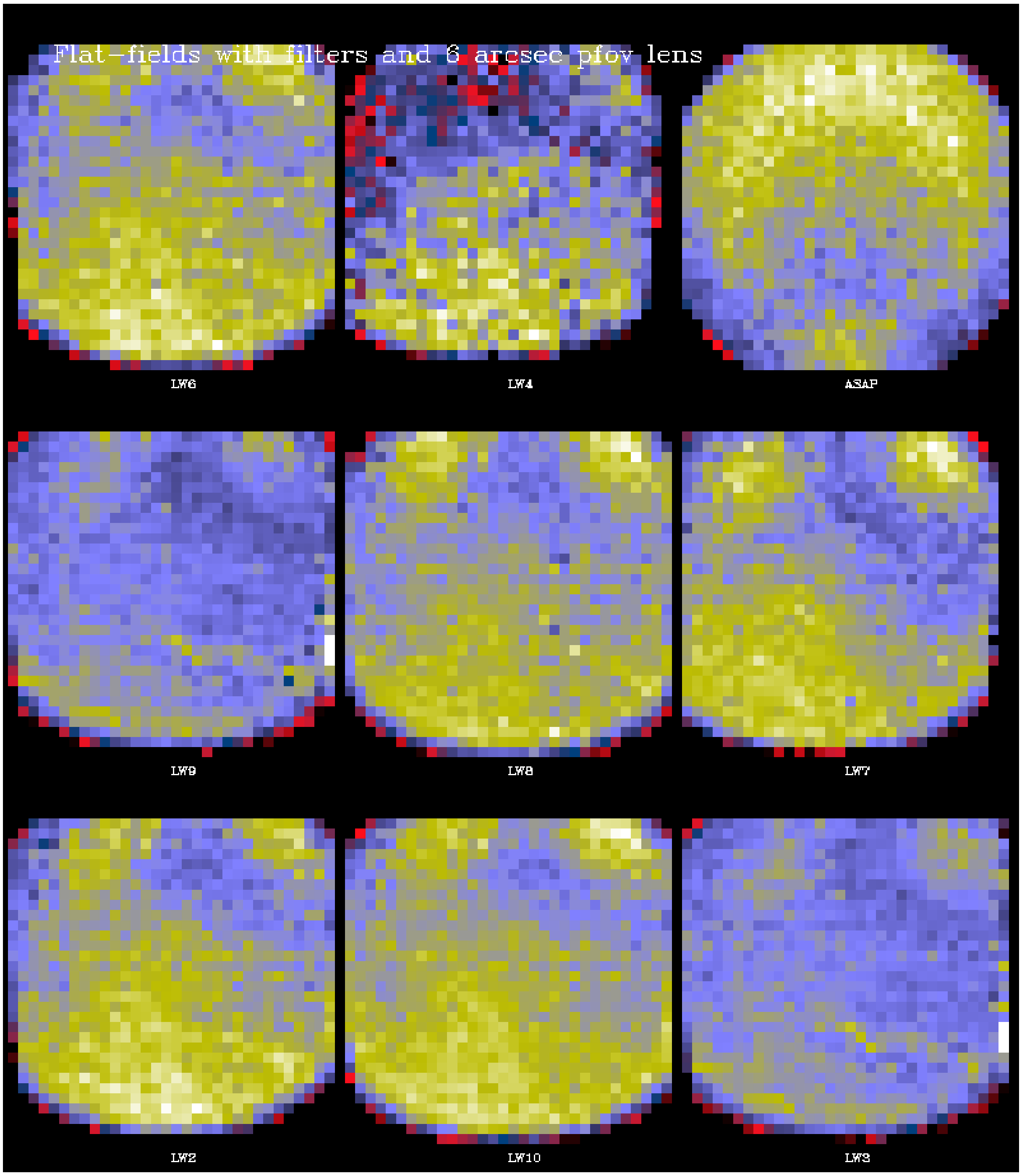

Figure 20: Comparison between measured and modeled optical flat-field for filters.

First idea on the ghost correction

Let I the observed image rearranged into a vector, S the sky it self rearranged also into a vector and C the convolution matrix. We can write:

$$I_i = \sum_j C_{ij} S_j \tag{1}$$

In the observation of a point source, the sky is approximated by a δ function and the uniform background emission B over the ISOCAM's filed-of-view. If $\delta_i(k)$ is the point source on the k-th pixel and b is the background level, the equation (1) is now written as:

$$I_i = \sum_j C_{ij}(\delta_j(k) + B_j) = C_{ik} + b \sum_j C_{ij}$$

If the ghost calibration observatins of the point source have been performed on a uniform background in the scale of ISOCAM's field-of-view, then the second term $b\Sigma_j C_{ij}$ corresponds to a flatfield scaled to the background level.

- A column of the convolution matrix is the background subtracted image of the observed point source located at k-th pixel.

- The matrix C_{ij} is obtained from the point source images and its corresponding flatfield image, only if we have these images for every k.

$\Rightarrow$ But: the calibration observations do not cover everything we need here and we have to replace the missing C_{ik} by an estimation obtained from interpolations.

Inversion

Once the convolution matrix C_{ij} is constructed, the most direct deconvolution method can be written as the inversion:

$$S_i = C_{ij}^{-1} I_j$$

which, as well known, does not work because the noise is amplified too much just like the point source in S_i seen as a Dirac function. However, an imposed final resolution R can reduce this noise:

$$R_{ij} S_i = R_{ij} C_{ij}^{-1} I_j = A_{ij} I_j$$

where $A_{ij} = (R_{ij} C_{ij}^{-1})$.

Imposed final spatial resolution

- As the goal of the deconvolution here is to correct for the ghosts and not to improve the spatial resolution, this final resolution can be set as large as the PSF width in the case of well sampled images (large PSF) and even larger than the PSF width for badly sampled images (PSF width smaller than 2×2 pixel size).

- In the second case the correction gives a worse spatial resolution, but this seems unavoidable unless a special noise supression algorithm is applied.

Preliminary result

- The major difficulty is to improve the interpolation method for the construction of the convolution matrix.

- This interpolation requires the separation of the point source and ghosts.

- In the case of CVF with 6 arcsec pixel field-of-view lense, the two main ghosts fall on the point source at the detector centre.

- The interpolation over the central region is of poor quality.

- The search for a better method of interpolation seems to be the unavoidable next step.

- Improve the computed PSF for the separation of the source and the ghosts?

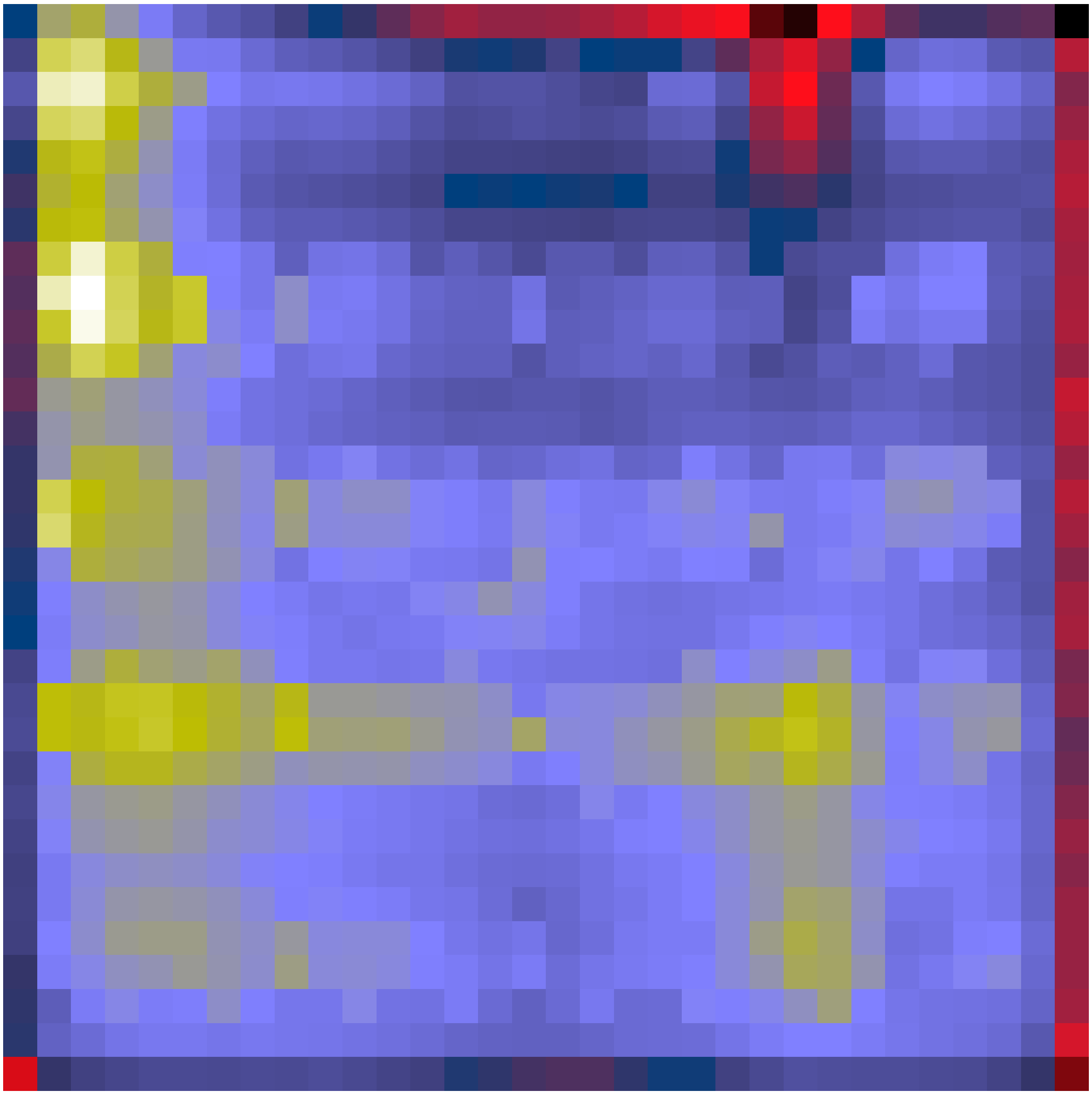

Figure 21: A CVF flatfield made by interpolating CVF point source data

Asymmetry of the PSFs

- Every PSF measurements show the asymmetry which is well noticed on the first ring

- An analysis of the pupil plane was made by mixing measured PSFs and their corresponding computed PSF

$$
\begin{array}{ll}
 & \left\{ \begin{array}{l} \sqrt{\text{measured PSF}} \\ \text{Computed phase} \end{array} \right. \\
\Rightarrow^{\text{FFT}} & \left\{ \begin{array}{l} \text{synthesized aperture amplitude} \\ \text{synthesized aperture phase} \end{array} \right. \\
\Rightarrow^{\text{FFT}^{-1}} & \left\{ \begin{array}{l} \text{synthesized PSF amplitude} \\ \text{synthesized PSF phase} \end{array} \right.
\end{array}
$$

- The result is to be further analysed and this MAY allow to include the asymmetry in the computation of PSFs

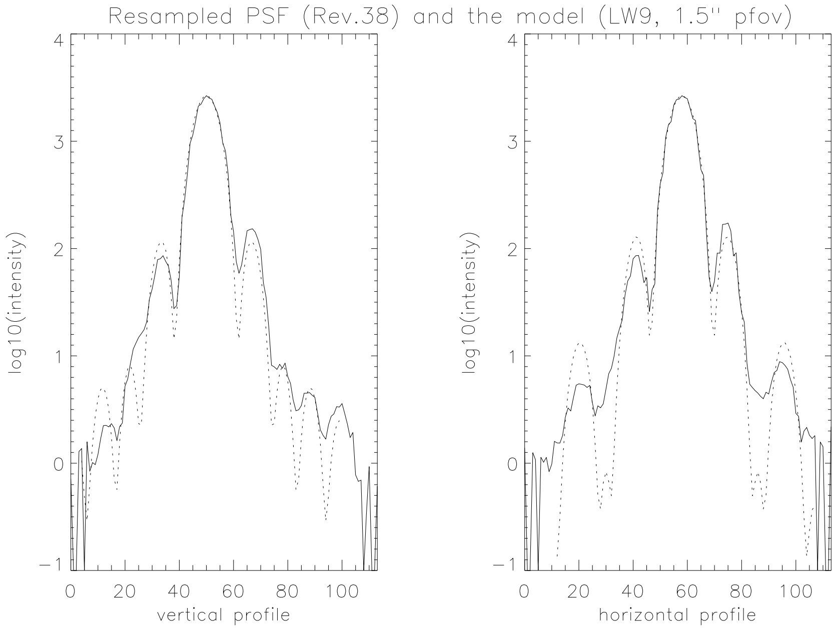

Figure 22: Comparison of measured PSF and modelled PSF with LW9 and 1.5 arcsec pfov

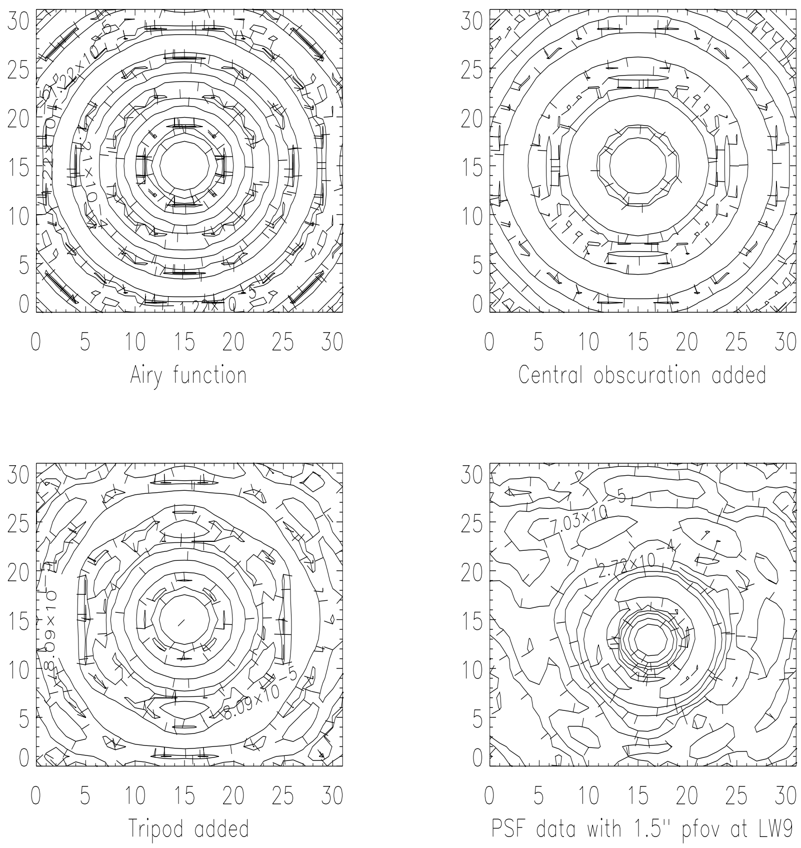

Figure 23: Comparison with modeled PSFs for 1.5 arcsec pfov at LW9 filter.

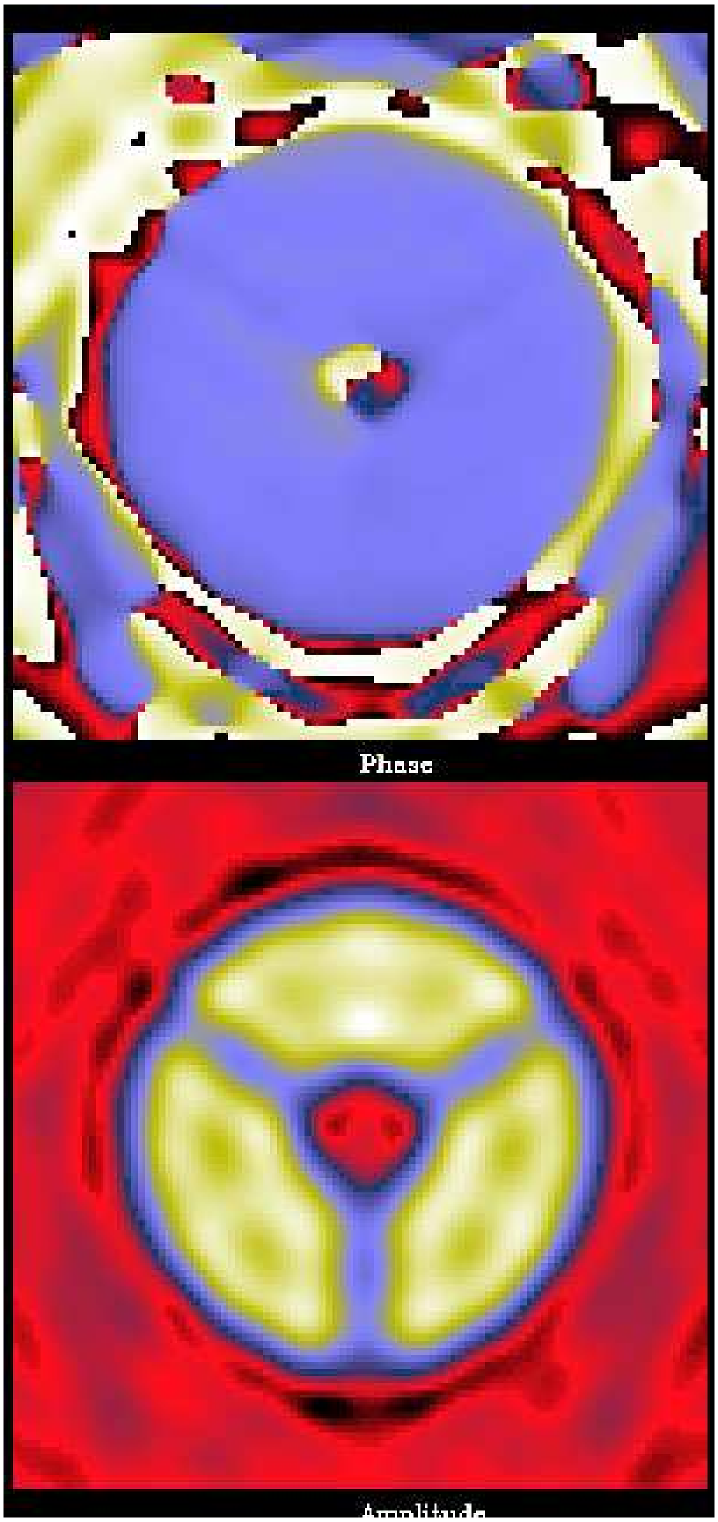

Figure 24: Synthesized complex aperture of 1.5 arcsec pfov at LW9

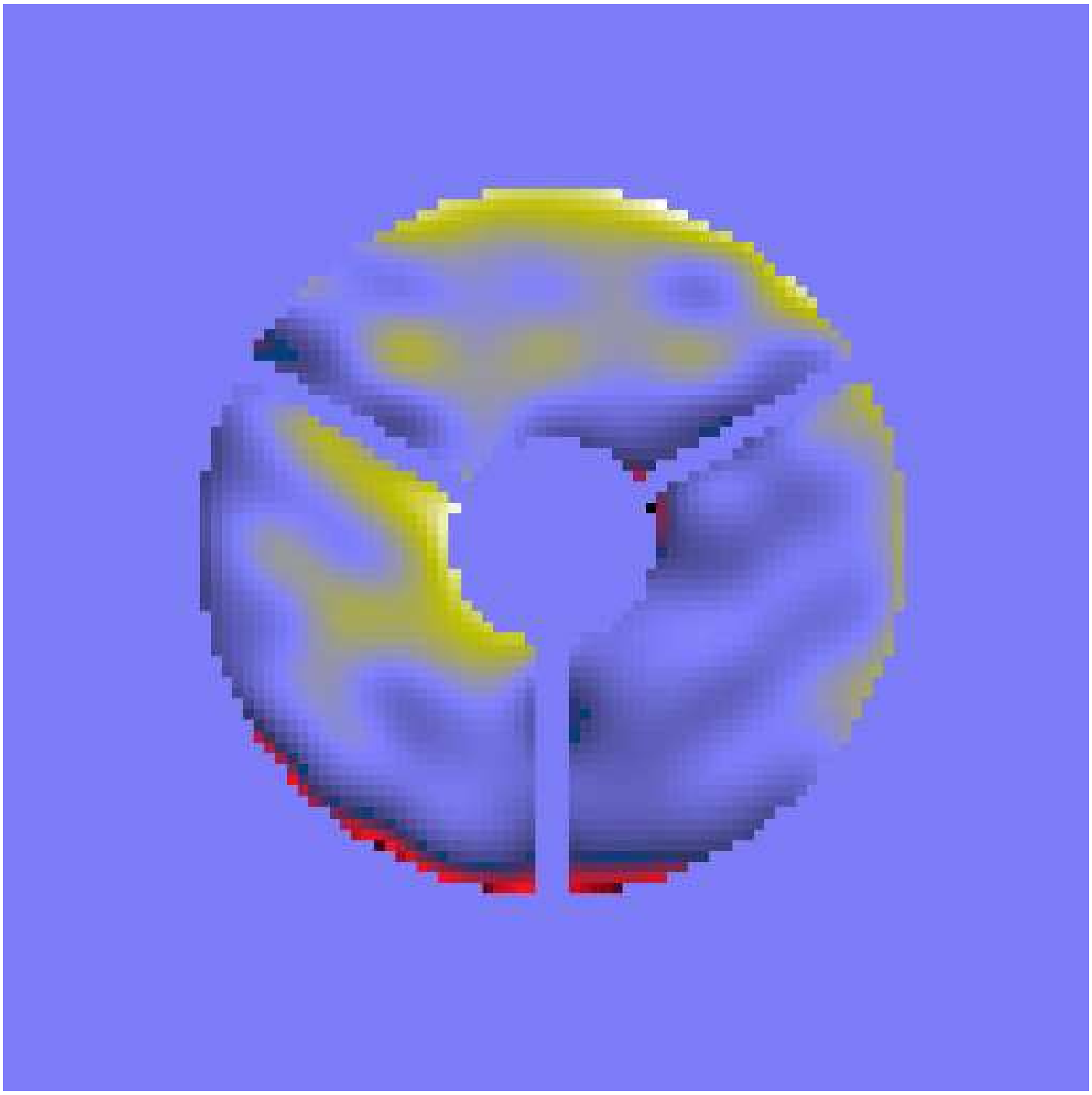

Figure 25: Phase inside the pupil of synthesized aperture

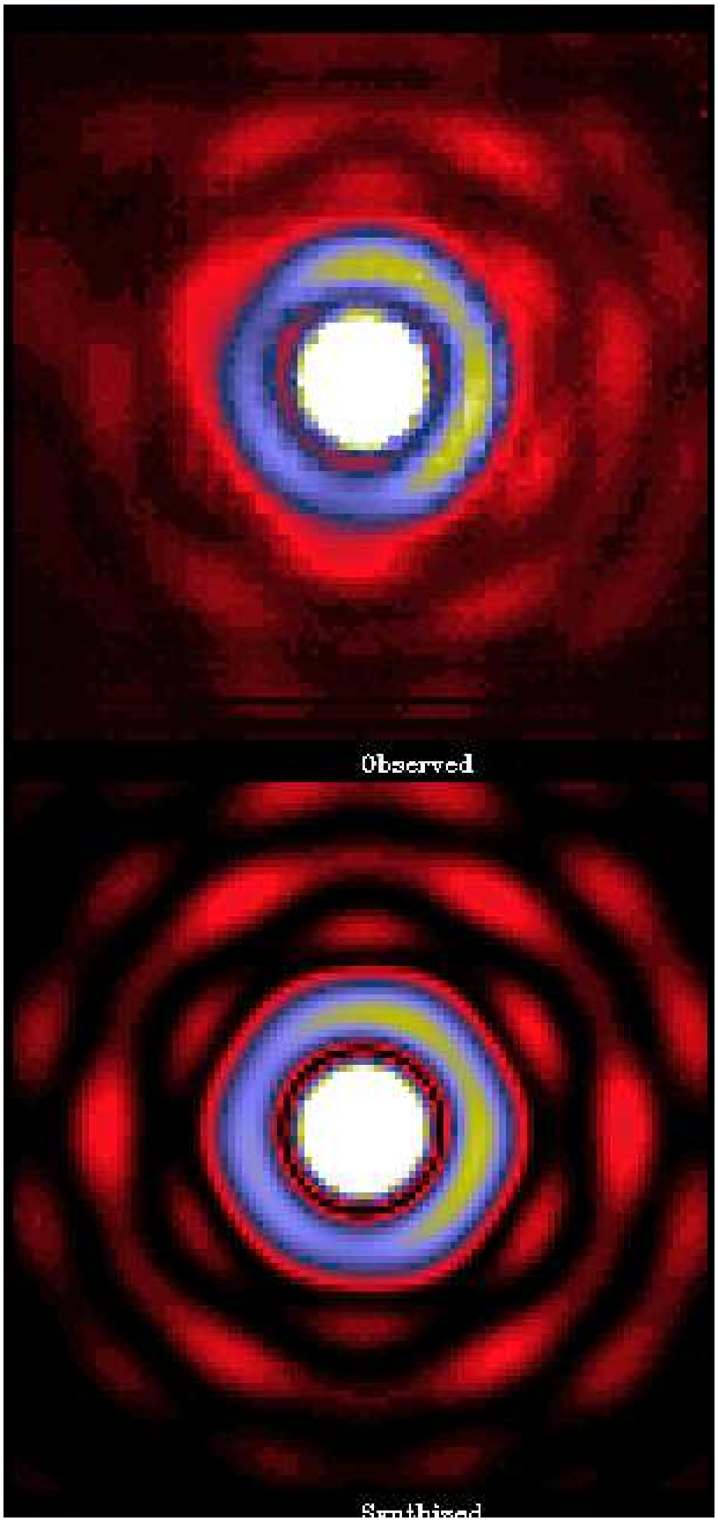

Figure 26: Observed and synthesized PSFs: 1.5 arcsec pfov at LW9